Hindawi Publishing Corporation
International Journal of Polymer Science
Volume 2016, Article ID 9104395, 9 pages
http://dx.doi.org/10.1155/2016/9104395

Research Article

Effects of Organomontmorillonite Content on Morphology and Mechanical and Thermal Properties of Poly(2,6-dimethyl-1,4-phenylene oxide)/Polyamide-66 Nanocomposites

Kunxiao Yang,[1] Chunling Xin,[1] Ying Huang,[1] Lilong Jiang,[1] and Yadong He[1,2]

[1]*College of Mechanical and Electrical Engineering, Beijing University of Chemical Technology, Beijing 100029, China*
[2]*The Engineering Research Center of Polymer Processing Equipment, Ministry of Education, Beijing 100029, China*

Correspondence should be addressed to Yadong He; heyd@mail.buct.edu.cn

Received 9 August 2016; Accepted 18 September 2016

Academic Editor: Xiao Gong

The nanocomposites consisting of polymer matrix and nanofiller have attracted great attention because of the improved physical properties. In this paper, organomontmorillonite (OMMT) was introduced into poly(2,6-dimethyl-1,4-phenylene oxide) grafted maleic anhydride (PPO-g-MA) compatibilized poly(2,6-dimethyl-1,4-phenylene oxide)/polyamide-66 (PPO/PA66) blends by melt extrusion. The morphology of PPO/PA66 nanocomposites with different amounts of OMMT was investigated using transmission electron microscopy (TEM), wide-angle X-ray diffraction (WAXD), and scanning electron microscopy (SEM). The OMMT platelets exhibited an exfoliated structure in the PA66 matrix and an intercalated structure on the surface of PPO domains at low OMMT loading (2 phr). However, the exfoliated platelets in matrix were found to transform into intercalated stacks by adding 6 phr of OMMT. The mechanical properties and thermal stability were significantly improved with the coexistence of exfoliated and intercalated OMMT at low OMMT loading (2–4 phr). The exfoliated OMMT platelets imposed a confinement effect on the macromolecular chains and thereby increased the storage modulus and complex viscosity of nanocomposites.

1. Introduction

Polymer/layered silicate nanocomposites have attracted great attention because of their ability to improve thermal stability and mechanical properties [1–5]. Organomontmorillonite (OMMT) is reported to be efficient in modifying the morphology of multiphase blends. Li et al. found that the selective localization of organ clays in the PA6 phase can change the viscosity ratio of multiphase polymer blends and prevent the coalescence of dispersed domains [6–8]. Since OMMT is a layered filler, separating the layer into intercalated or exfoliated structures is vital for property improvement [9, 10]. Moreover, the shape of nanoparticles shows a significant effect on the rheology and strength of nanocomposites [11, 12]. The microstructure of nanocomposites, especially for multiphase blends, depends drastically on the surface modification of filler and presence of compatibilizer. Therefore, functional groups are utilized to modify the surface of montmorillonite for higher layer spacing [13, 14].

In this study, OMMT is introduced to improve the mechanical and thermal properties of poly(2,6-dimethyl-1,4-phenylene oxide)/polyamide-66 (PPO/PA66) blends. The PPO/PA66 blends inherit the high chemical resistance and processability of PA66 and maintain the dimensional stability and good thermal properties of PPO. However, PPO/PA66 blends are restricted by high immiscibility due to the high interfacial tensions and the large differences in polymer polarities [15–19]. The properties of PPO/PA66 blends are strongly decided by the morphology and interfacial adhesion. However, the high viscosity ratio and incompatibility endow PPO/PA66 blends with poor mechanical properties with the absence of additives. Reactive compatibilization is an efficient way to strengthen interaction between components and to obtain blends or composites with desirable properties [20, 21].

PA66/PPO blends with smaller particle size and better mechanical properties could be prepared with the addition of copolymers containing maleic anhydride (MA) or glycidyl methacrylate (GMA) [22–26]. Moreover, the rigidity of both components necessitates the introduction of elastomers and rubbers into PPO/PA blends, such as styrene-butylene-styrene block copolymer (SBS), styrene-ethylene-butylene-styrene block copolymer (SEBS), and ethylene-propylene-diene terpolymer (EPDM) [27, 28]. Unfortunately, the toughened blends are restricted by low strength and low thermal stability, which are undesirable for engineering application [29–31].

In this work, PPO/PA66/OMMT nanocomposites were prepared with PPO grafted with MA (PPO-g-MA) serving as a compatibilizer and SEBS as an impact modifier. The relationship between OMMT loading and its microstructure was investigated via wide-angle X-ray diffraction and transmission electron microscope. The effects of compatibilizer on morphological structure of nanocomposites were further discussed. The main objectives of this study were to investigate the effects of OMMT dispersion on phase morphology, mechanical properties, thermal stability, and rheological properties of PPO/PA66/OMMT nanocomposites.

2. Experimental

2.1. Materials. PPO (LXR45) and PA66 (EPR27) were purchased from Shenma Industrial Co. and China National Bluestar Co., respectively. SEBS (Kraton G1651) was made by Shell Chemical Co., which contains 29 wt% styrene and number-averaged molecular weight of 29,000 in the PS blocks and 116,000 in the EB block. MA and dicumyl peroxide (DCP) (analytical grade reagents) were supplied by Beijing Chemical Industry Group Co. Organomontmorillonite (Nanocor I.34 TCN, density 52.00 g/cm^3) was modified with methyl dihydroxyethyl hydrogenated tallow ammonium.

2.2. Sample Preparation. PPO was grafted with MA as compatibilizer via reactive melt extrusion. Briefly, powders of PPO, MA, and DCP were premixed at a ratio of 100/2/0.1 in a homogenizer at 70°C for 10 min. The mixture was extruded by a Coperion twin-screw extruder (ZSK 26 Mc) at 180/260/270/290/290/290/290/280°C and a screw speed of 120 rpm. This graft reaction was studied by Fourier transform infrared spectrometry (FTIR) analysis and titration analysis. The grafted MA content in PPO-g-MA was about 0.5–0.6 wt%.

All the materials were dried at 80°C for 12 h and premixed for 5 min before extrusion. The melt compounding was carried out on a self-designed trangle with a screw diameter of 35.2 mm and a length-diameter ratio (L/D) of 28. The screw speed was maintained at 200 rpm and the barrel temperature was 240–285°C. Moreover, the compatibilized ternary blend (PPO/PPO-g-MA/PA66/SEBS = 25/25/50/5; marked as T) and nanocomposites with different OMMT contents (PPO/PPO-g-MA/PA66/SEBS/OMMT = 25/25/50/5/x; marked as N-x) were prepared for comparison. The extruded blends or nanocomposites were dried in a vacuum oven at 80°C for 8 h and then molded into standard specimens by a HAITIAN SA900/260 injection molding machine, which operated at the barrel temperature of 270/280/285/290/280°C and injection pressure of 60 MPa.

2.3. Characterization. Pure OMMT, N-2, N-4, and N-6 were characterized on an Empyrean wide-angle X-ray diffractometer (WAXD; PANalytical, Netherlands) at $\lambda = 0.154$ nm, 4 kW, 2θ = 1–30°. The scanning speed was 5°/min with a step of 0.025°.

The dispersion of OMMT in blends was investigated using a Hitachi H-800 transmission electron microscope (TEM) at an accelerating voltage of 200 kV. The nanocomposites were ultramicrotomed to ~100 nm thick samples using a LECIA EMUC7. The samples were stained by osmium tetroxide (OsO_4) for 30 min.

The morphology was observed under a Quanta 250 FEG scanning electron microscope (SEM). All the injected samples were kept in liquid nitrogen for some time and brittle-fractured. The surfaces were etched in chloroform over 8 h for selective dissolution of PPO. Moreover, some of the samples were etched with boiled n-hexane for 3 h for removal of SEBS phase. The etched surfaces were kept in vacuum at 80°C for 8 h and then gold-coated before observation. The number-averaged particle diameter $\overline{D_n}$ and volume average particle size $\overline{D_v}$ of the dispersed phase were analyzed with an image analyzer (*Image J 1.41*) and calculated according to the following:

$$\overline{D_n} = \frac{\sum N_i D_i}{\sum N_i},$$
$$\overline{D_v} = \frac{\sum N_i D_i^4}{\sum N_i D_i^3}, \quad (1)$$

where N_i is the number of particles with diameter D_i. The number of particles in this study was 300–400 per sample.

Notched impact strengths (ISO-179-2010) were measured using a pendulum impact tester (ZBC 1400-2, Shenzhen Sans Co.) at room temperature, and the impact energy was 4 J. The tensile (ISO-8256-2005) and flexural (ISO-178-2010) properties were measured with a universal testing instrument (XWW, Chengde Jinjian Co.) at a crosshead speed of 50 mm/min and 2 mm/min, respectively.

Dynamic mechanical thermal properties of nanocomposites were investigated using a DMA 242 (Netzsch, Germany), with a specimen dimension of 16 × 12 × 5 mm^3. The sample was heated from −20°C to 250°C at a heating rate of 3°C /min. A frequency of 1 Hz was used after optimization of the static and dynamic forces.

Thermogravimetric analysis (TGA) was performed under nitrogen flow from 40 to 800°C with heating rate of 10°C /min by using a TA TGA Q50 thermal analyzer.

Dynamic rheological properties of nanocomposites were determined with a HAAKE MARS-III rotational rheometer (parallel-plate geometry; diameter = 20 mm; gap = 1 mm) in a nitrogen environment. Frequency sweeping was performed at 280°C at a frequency range of 0.01–100 s^{-1}, with a strain of 1%.

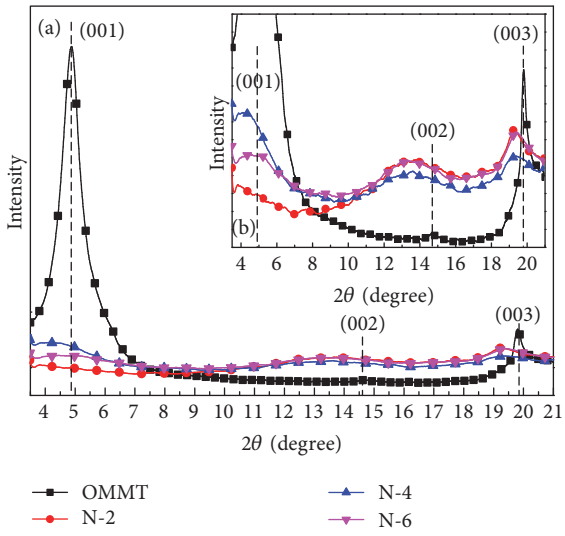

FIGURE 1: WAXD patterns of OMMT and nanocomposites N-2, N-4, and N-6: (a) original patterns; (b) magnified patterns.

3. Results and Discussion

3.1. Dispersion of OMMT in PPO/PA66. The location and dispersion of OMMT in multiphase blends are vital for property improvement of nanocomposites. The exfoliation and microstructure of OMMT in PPO/PA66 blends were investigated via WAXD and TEM.

WAXD patterns of OMMT and its nanocomposites are shown in Figure 1. The peak (001) and its higher order diffractions, for example, (002) and (003), of pure OMMT (dashed line in Figure 1) are at $2\theta = 4.91, 14.67, 19.80^{\circ}$, respectively, which correspond to basal spacing of 1.80, 0.60 and 0.44 nm, respectively, according to Bragg's law ($\lambda = 2d \sin\theta$, where d is the layer spacing; λ is the X-ray wavelength). Compared with pure OMMT, the (001) peaks of nanocomposites N-2, N-4, and N-6 all shift leftward to a lower angle (about 4°), while the corresponding d increases to 2.2 nm. For each nanocomposite, d of the (002) and (003) peaks increases to 0.65 nm ($2\theta = 13.73^{\circ}$) and 0.46 nm ($2\theta = 19.25^{\circ}$), respectively. It is indicated that some molecular chains are intercalated between the stacked OMMT layers, so intercalated composites are obtained. These phenomena are attributed to the strong affinity between the anhydride group and OMMT surface and/or the hydroxyl groups of PPO and the ammonium surfactant [32–34]. Furthermore, this result may be caused by the separation of OMMT galleries under the shear flow of extruder. However, the gallery spacing is reduced with the increase of OMMT concentration. For N-6, a broad (001) peak appears around 4.5°, corresponding to 1.91 nm. The reason is that the polymer-OMMT interactions at high clay concentration are dominated by the van der Waals force, which limits the expansion of OMMT galleries [9]. Meanwhile, the preservation of the three diffraction peaks indicates that a significant amount of OMMT remained in the layered form after melt extrusion.

To further explore the dispersion of OMMT and the microstructure of nanocomposites, we investigated the morphologies of N-2, N-4, and N-6 using TEM (Figure 2). The dark line is the stack of OMMT platelet and the dark part with small domains is the PPO phase, while the matrix is the PA66 phase. At the loading of 2 phr of OMMT, it is noteworthy that silicates are located at both the PA66 matrix and the PPO-PA66 interfaces. In the PA66 matrix, OMMT shows a disruption of platelet with a uniform platelet separation. This indicates an exfoliated structure of OMMT platelets. Moreover, the platelets exhibit an intercalated structure on the surface of PPO/PA66 blends. These results suggest that the intercalated structure and the exfoliated structure coexist and are selectively located in nanocomposites (Figure 3). With PPO-g-MA as the compatibilizer, the strong affinity between MA group and OMMT surface makes the intercalated silicates locate at the PPO-PA66 interfaces [32, 33]. Due to the barrier effect of the interfacial platelets, the OMMT could effectively prevent the coalescence of dispersion.

When the OMMT loading increases to 4 phr, a similar dispersion of OMMT was observed, and a bit of small stacks appeared in the PA66 matrix. This phenomenon indicated that the surface of the PPO droplets was saturated with the OMMT platelets. At high OMMT concentration (N-6), the number of stacks in the matrix increased apparently. The exfoliated OMMT platelets were found to transform into intercalated stacks in PA66 matrix. These agglomerates of OMMT could cause premature fracture in mechanical test which is discussed in Section 3.2.

3.2. Morphology of the Nanocomposites. Figure 4 illustrates the morphologies of the etched fracture surfaces of PPO/PA66 blend and its nanocomposites. The black domains indicate the extracted PPO phase. With PPO-g-MA as an effective compatibilizer, the interfaces between PPO and PA66 in blend T are vague and uneven. Nevertheless, the PPO domain has a wide particle size distribution, which is attributed to the high viscosity ratio of PPO/PA66. Compared with blend T (D_n = 0.79 μm), the nanocomposites N-2, N-4, and N-6 show smaller PPO domains (0.65, 0.61, and 0.69 μm, resp.). However, the PPO domain size is not significantly affected by the increase of OMMT loading.

These phenomena are attributed to the variation of OMMT distribution and location on the morphology of PPO/PA66 blends. As OMMT exhibited exfoliated structure in the PA66 matrix, the viscosity ratio of PPO/PA66 decreases significantly, which is beneficial for the breakdown of dispersed droplets [32]. Moreover, the interfacial presence of intercalated OMMT exerts a barrier effect (Figure 3), which prevents the coalescence of PPO domains. As for nanocomposite N-6, the thick OMMT stacks play a limiting role in preventing the coalescence of dispersion, so the domain size of PPO increases at high OMMT loading.

3.3. Mechanical Properties. The mechanical properties of polymer blends are dominated by their morphological structures. The relationship between notched impact strengths and particle size with increasing OMMT content is shown in Figure 5. The impact strength of nanocomposites is first

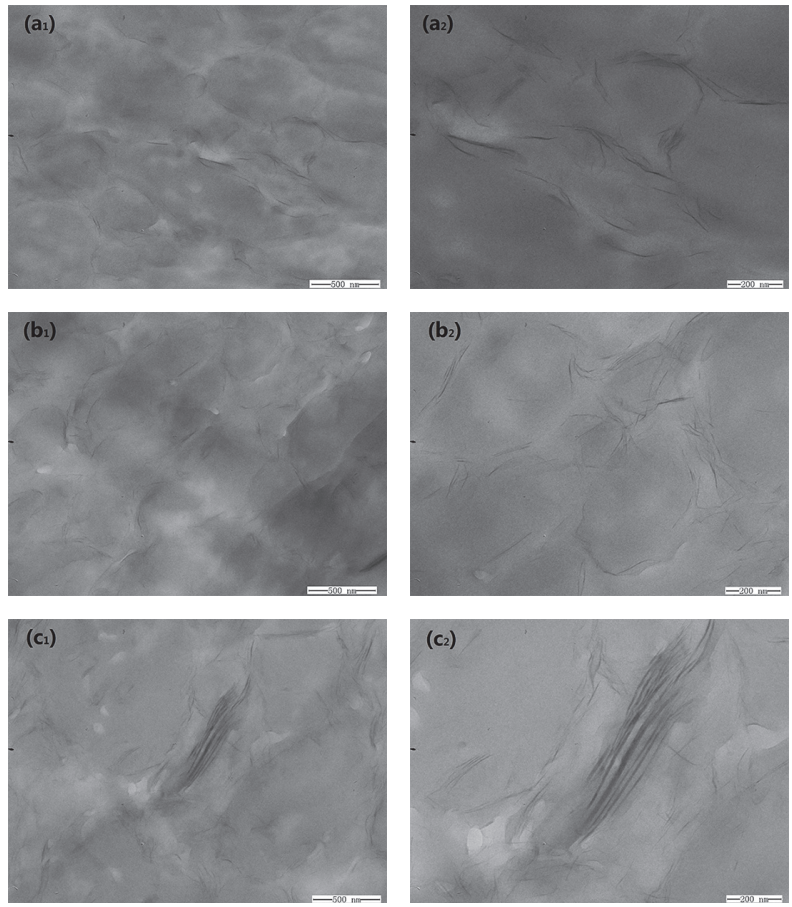

Figure 2: TEM micrographs of PPO/PA66 nanocomposites: (a_1) N-2; (a_2) high magnification of (a_1); (b_1) N-4; (b_2) high magnification of (b_1); (c_1) N-6; (c_2) high magnification of (c_1).

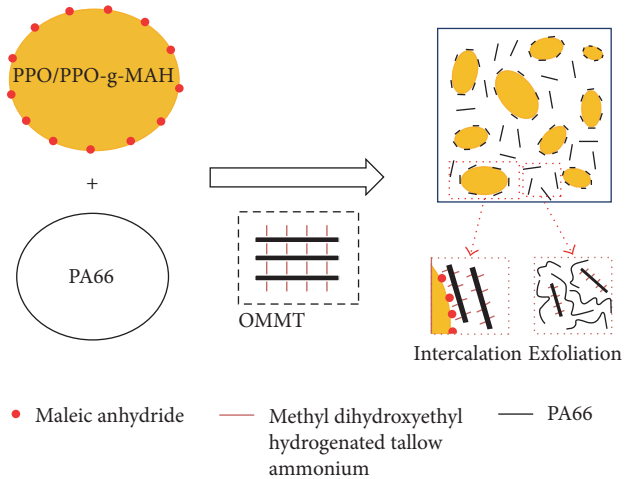

Figure 3: Schematic diagram for dispersion of OMMT in PPO/PA66 nanocomposite.

improved and then weakened dramatically with the increase of OMMT content. This phenomenon is attributed to the changes of OMMT morphology and droplet diameter, by which the smaller particle size could significantly enhance the multiphase interaction and reduce the stress concentration in blends. Nevertheless, with the increase of OMMT loading (N-6), the appearance of OMMT stacks in the PA66 matrix aggravates the stress concentration which would accelerate the fracture in impact test.

As shown in Figure 6, both tensile strength and flexural strength are sharply improved with the addition of OMMT. This improvement is due to the exfoliated OMMT which increases the rigidity of the PA matrix. However, the tensile strength of nanocomposites decreased dramatically at high OMMT loading. The reason is that the presence of OMMT stacks in PA66 matrix would induce defects during tensile tests, resulting in the decrease of tensile strength. These phenomena illustrate that the dispersion of OMMT significantly affects the mechanical properties.

For modification of PPO/PA66 blends, it is difficult to keep a balance between the toughness and strength of the immiscible system. In this study, the impact strength, tensile strength, and flexural strength of PPO/PA66 composites are all significantly improved with an appropriate addition of OMMT. To further explore the effect of OMMT morphology on mechanical properties improvement, we observed the morphology of brittle-fractured surfaces of N-2 etched by

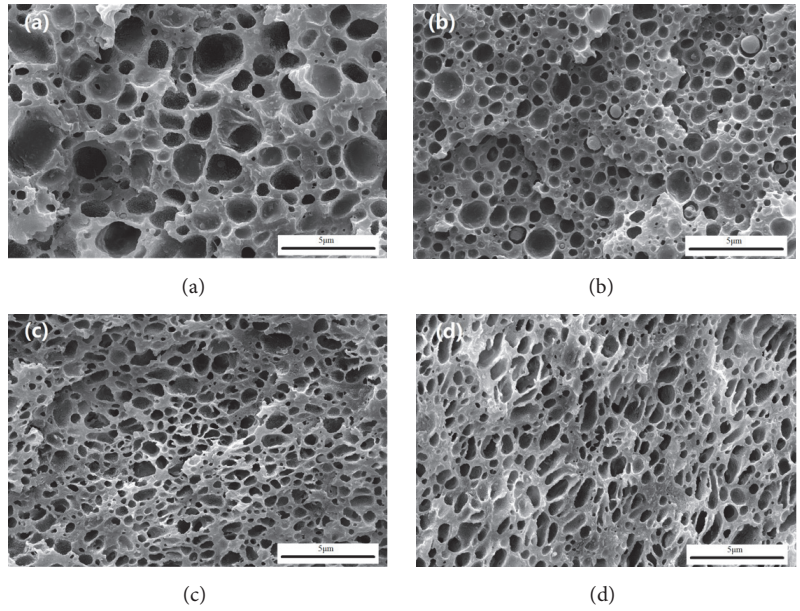

Figure 4: SEM micrographs of PPO/PA66 blends and nanocomposites: (a) T; (b) N-2; (c) N-4; (d) N-6.

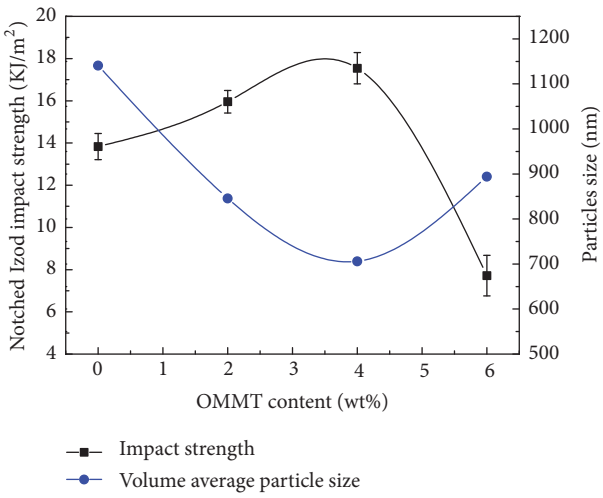

Figure 5: The relation of notched impact strengths and particle size for PPO/PA66 nanocomposites.

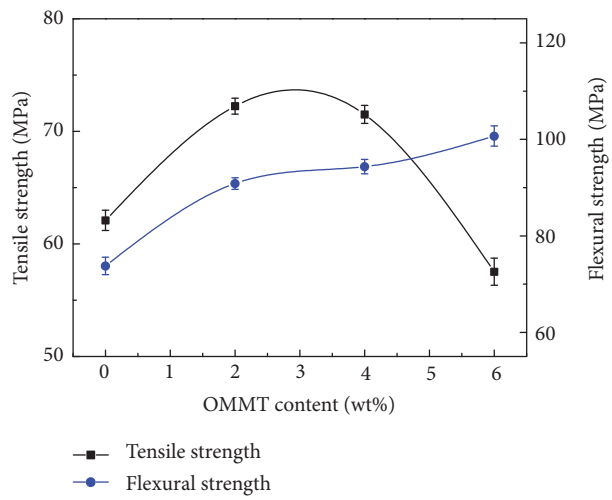

Figure 6: Tensile strengths and flexural strengths of PPO/PA66 nanocomposites with addition of OMMT.

n-hexane, which could selectively remove the SEBS phase. As shown in Figure 7, SEBS is mainly located in the PPO phase, which is ascribed to the high compatibility between PS block and PPO. According to a previous study, the PPO/SEBS (90/10) blend has excellent impact strength of 33.5 KJ/m^2, which indicates that the dispersed domains act as toughened particles in toughening of PA66 matrix. Meanwhile, the polar OMMT is highly affinitive to both polar PA66 and the MA group in the PPO phase [7, 32]. Thus, the intercalated OMMT at the PPO-PA66 interface could enhance the interfacial adhesion and reduce the phase separation, thereby improving the impact strength. Furthermore, the exfoliated OMMT leads to a confinement effect to PA66 chains, which

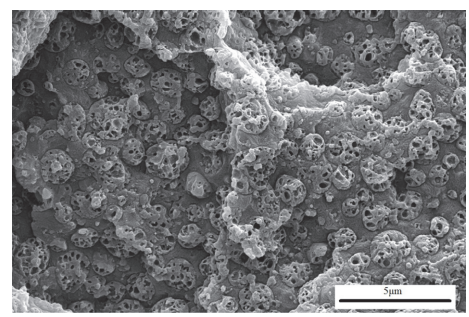

Figure 7: SEM micrographs of brittle-fractured surfaces of nanocomposite N-2 etched by n-hexane.

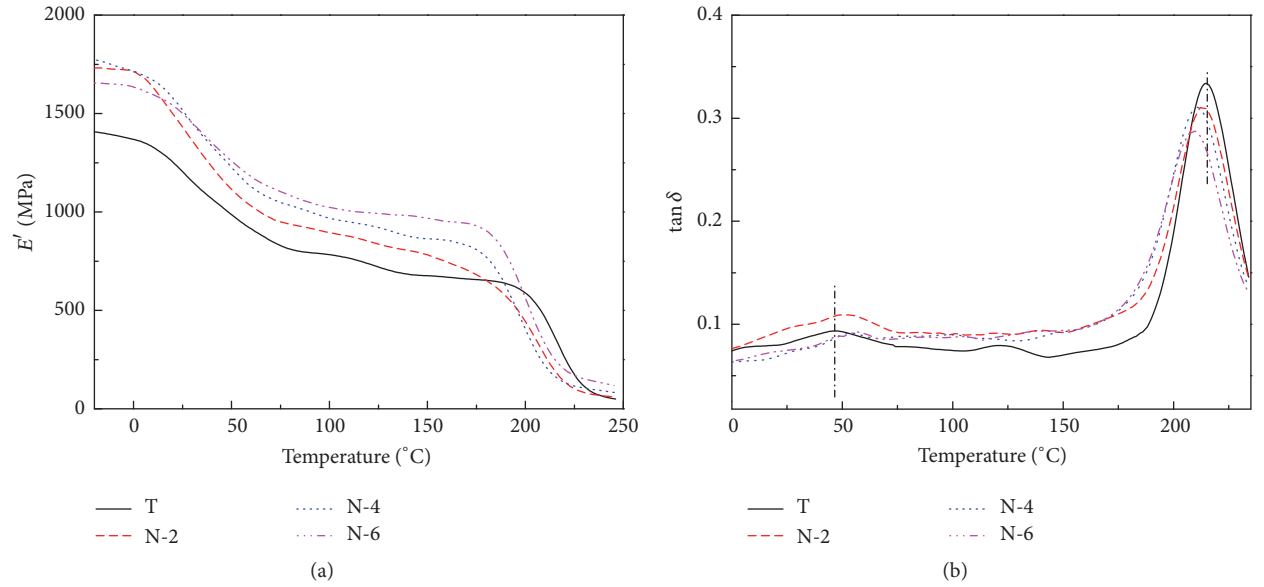

Figure 8: (a) Storage modulus (E') and (b) loss factor ($\tan\delta$) patterns of DMTA for PPO/PA66 blends and nanocomposites.

Table 1: The data of DMTA for PPO/PA66 blend and nanocomposites.

Sample	E' (Mpa, 0°C)	E' (Mpa, 150°C)	T_g (°C)	
			PA66	PPO
T	1368.6	675.8	48.4	222.8
N-2	1712.8	781.8	51.8	213.4
N-4	1714.7	863.9	53.6	210.6
N-6	1635.1	968.6	52.2	209.4

Table 2: Thermal data of PPO/PA66 blend and nanocomposites.

Sample	$T_{onset\,(5\%)}$ (°C)	T_{max} (°C)	Residue at 600°C (wt%)
T	452.8	391.6	1.71
N-2	455.8	397.5	7.75
N-4	457.5	396.8	9.78
N-6	459.8	400.6	11.56

enhances the rigidity of PA matrix. Therefore, the synergistic effect between the intercalated structure and the exfoliated structure in nanocomposites could efficiently improve both toughness and strength.

3.4. Thermal Properties. The effect of OMMT on nanocomposite was investigated through dynamic mechanical thermal analysis (DMTA) and thermogravimetric analysis. Figure 8(a) illustrates the temperature dependence of storage modulus (E') for PPO/PA66 blends and nanocomposites. Two distinct decreases of E' occur with the temperature rise, corresponding to the chain segment relaxation of PA66 and PPO, respectively. The nanocomposites exhibit significantly higher E' than PPO/PA66 blends over the test temperature range (−20 to +250°C) (Table 1). This result indicates that the addition of OMMT reinforces both PA66 and PPO phases, as the exfoliated and intercalated OMMT platelets impose a significant constraint on the mobility of the PA66 and PPO chain segments. However, E' of nanocomposite N-6 is lower than those of N-2 and N-4 in the low temperature region, indicating a decrease in rigidity of PA66 phase. It proves that the presence of OMMT agglomerates induces defects in PA66 matrix.

The loss factors ($\tan\delta$) of PPO/PA66 blends and nanocomposites are shown in Figure 8(b). All samples have two major peaks corresponding to the glass transition temperatures (T_g) of PA66 and PPO phases, respectively. The peaks shift towards each other with the increase of OMMT loading, which implies the improved compatibility between the two phases. It is indicated that the higher OMMT loadings of nanocomposites generate a higher volume of constrained polymers, despite the greater exfoliation in lower-OMMT samples.

The TGA data were analyzed to determine if the thermal stability and thermal degradation were influenced by the dispersion of OMMT. As shown in Figure 9, the addition of OMMT is favorable for thermal properties of PPO/PA66/OMMT nanocomposites. The presence of OMMT resists against the destructive effect of high temperature on macromolecular chains. Moreover, the thermal stability of nanocomposites is improved gradually with the increase of OMMT loading, which implies the type of dispersion has no significant effect on the thermal properties. Some representative TGA data are listed in Table 2.

3.5. Rheological Properties. The storage modulus (G') and complex viscosity (η^*) of PPO/PA66 blend and its nanocomposites against the shear rate are shown in Figure 10. For

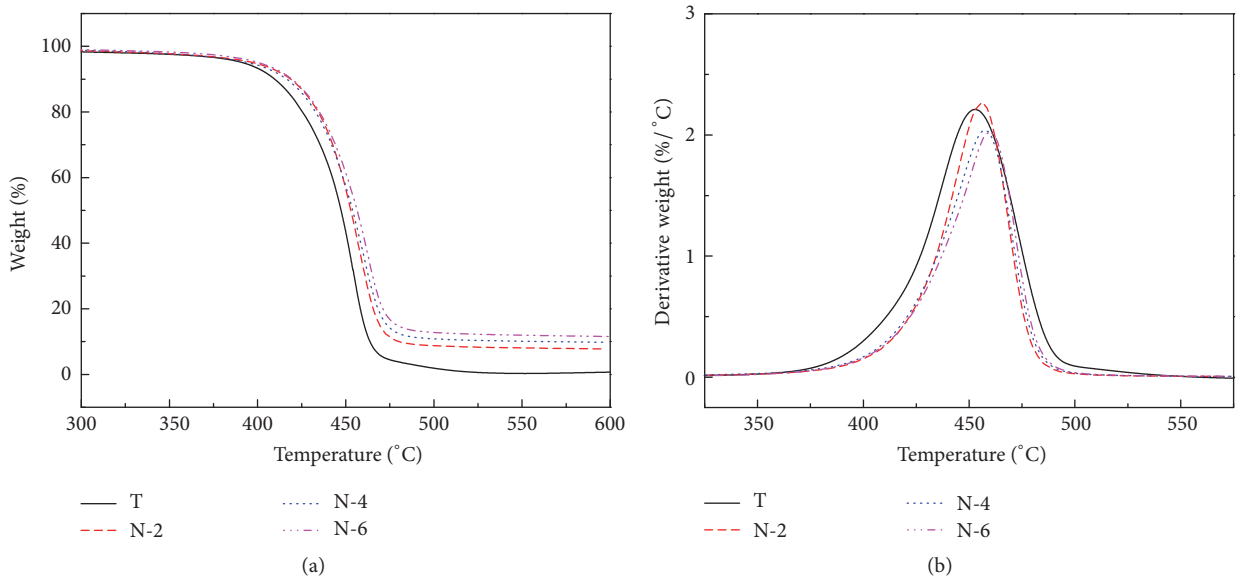

Figure 9: (a) TGA decomposition and (b) derivative TGA curves of PPO/PA66 blends and nanocomposites.

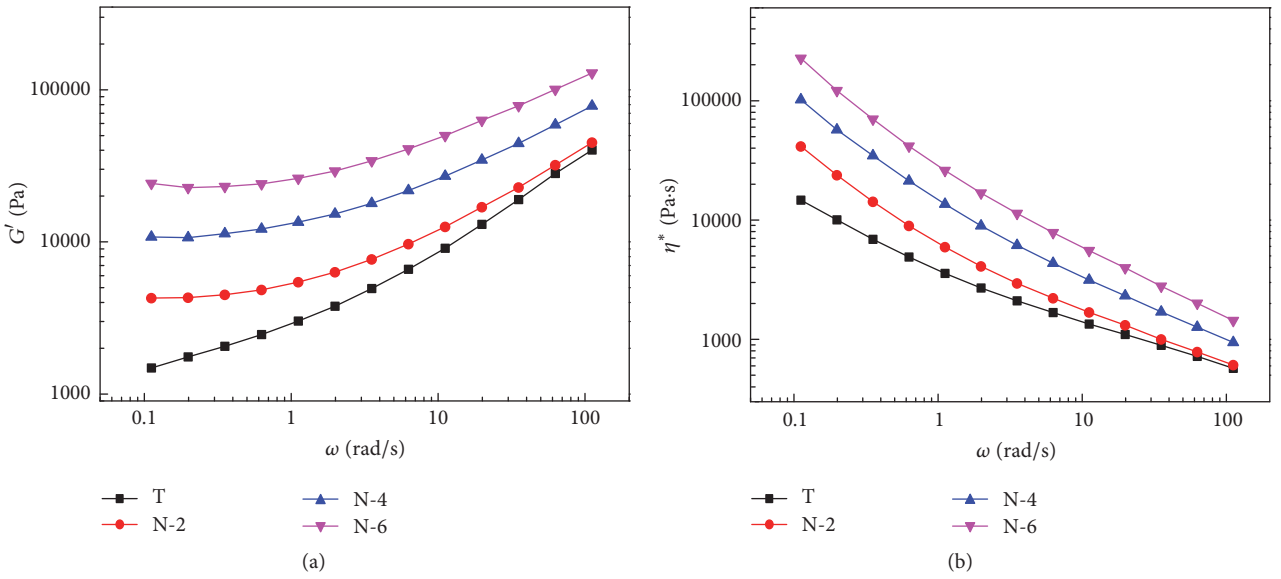

Figure 10: (a) Storage modulus (G') and (b) complex viscosity (η^*) patterns of PPO/PA66 blends and nanocomposites.

PPO/PA66 blends, G' and η^* both are increased with the addition of OMMT, especially at low frequencies. Generally, the higher G' and η^* correspond to a slower relaxation of the macromolecular chains, which is consistent with the analysis of thermal mechanical properties. The exfoliation of OMMT platelets could change the microstructure of nanocomposites, leading to a sensitive response in the dynamic rheological behavior. Moreover, the viscosity of N-2 is nearly overlapped with that of the OMMT-free sample T at high shear rate, which could significantly improve the mechanical properties. It means that PPO/PA66 blends with the coexistence of exfoliated and intercalated OMMT could maintain both mechanical properties and processability.

4. Conclusions

OMMT was introduced into PPO/PA66 blend to prepare nanocomposites with excellent mechanical properties by simple melt compounding. Under appropriate loading (2, 4 phr), OMMT shows an exfoliated structure in PA66 matrix and an intercalated structure at the PPO-PA66 interfaces with the presence of PPO-g-MA. This special microstructure lessens the dispersed particle diameter and improves the interfacial adhesion, thus significantly enhancing both toughness and strength. At high OMMT loading (6 phr), the presence of OMMT agglomerates limits the mechanical properties of PPO/PA66 composites. The addition of OMMT

also improves the thermal mechanical properties and thermal stability, thus expanding the engineering application of the nanocomposites. The homogeneous exfoliated or intercalated structure of OMMT significantly constrains the mobility of both PA66 and PPO chain segments, thus increasing the viscosity of nanocomposites. Overall, since the comprehensive properties of PPO/PA66/OMMT nanocomposites are significantly improved with the addition of OMMT, the optimum content of OMMT is 2 to 4 phr.

Competing Interests

The authors declare that the received funding from National Natural Science Foundation of China leads to no conflict of interests regarding the publication of this paper.

Acknowledgments

The authors gratefully acknowledge the support from the National Natural Science Foundation of China (Project no. 51273019).

References

[1] B. Han, G. Ji, S. Wu, and J. Shen, "Preparation and characterization of nylon 66/montmorillonite nanocomposites with co-treated montmorillonites," *European Polymer Journal*, vol. 39, no. 8, pp. 1641–1646, 2003.

[2] R. Gallego, D. García-López, J. C. Merino, and J. M. Pastor, "The effect of montmorillonite and compatibilizer quantities on stiffness and toughness of polyamide nanoblends," *Polymer International*, vol. 59, no. 4, pp. 472–478, 2010.

[3] Y. Wu, Y. Shi, L. Zhu, B. Shentu, and Z. Weng, "Joint effect of compatibilizer and organo-montmorillonite on compatibilization of polyamide-6/poly(phenylene oxide) blend: morphology and properties," *Polymer-Plastics Technology and Engineering*, vol. 54, no. 7, pp. 682–690, 2015.

[4] Kusmono, Z. A. Mohd Ishak, W. S. Chow, T. Takeichi, and Rochmadi, "Compatibilizing effect of SEBS-g-MA on the mechanical properties of different types of OMMT filled polyamide 6/polypropylene nanocomposites," *Composites Part A: Applied Science and Manufacturing*, vol. 39, no. 12, pp. 1802–1814, 2008.

[5] X. Gong, Y. Bao, C. Qiu, and C. Jiang, "Individual nanostructured materials: fabrication and surface-enhanced Raman scattering," *Chemical Communications*, vol. 48, no. 56, pp. 7003–7018, 2012.

[6] M. Sabard, F. Gouanvé, E. Espuche et al., "Influence of montmorillonite and film processing conditions on the morphology of polyamide 6: effect on ethanol and toluene barrier properties," *Journal of Membrane Science*, vol. 450, pp. 487–498, 2014.

[7] Y. Li and H. Shimizu, "Novel morphologies of poly(phenylene oxide) (PPO)/polyamide 6 (PA6) blend nanocomposites," *Polymer*, vol. 45, no. 22, pp. 7381–7388, 2004.

[8] Y. Li and H. Shimizu, "Co-continuous polyamide 6 (PA6)/Acrylonitrile-Butadiene-Styrene (ABS) nanocomposites," *Macromolecular Rapid Communications*, vol. 26, no. 9, pp. 710–715, 2005.

[9] A. Ranade, N. A. D'Souza, and B. Gnade, "Exfoliated and intercalated polyamide-imide nanocomposites with montmorillonite," *Polymer*, vol. 43, no. 13, pp. 3759–3766, 2002.

[10] M. Motovilin, Z. Denchev, and N. Dencheva, "On the structure-properties relationship in montmorillonite-filled polyamide 6 nanocomposites," *Journal of Applied Polymer Science*, vol. 120, no. 6, pp. 3304–3315, 2011.

[11] S. T. Knauert, J. F. Douglas, and F. W. Starr, "The effect of nanoparticle shape on polymer-nanocomposite rheology and tensile strength," *Journal of Polymer Science, Part B: Polymer Physics*, vol. 45, no. 14, pp. 1882–1897, 2007.

[12] T. Xu and V. A. Davis, "Liquid crystalline phase behavior of silica nanorods in dimethyl sulfoxide and water," *Langmuir*, vol. 30, no. 16, pp. 4806–4813, 2014.

[13] X. Kornmann, H. Lindberg, and L. A. Berglund, "Synthesis of epoxy-clay nanocomposites: influence of the nature of the clay on structure," *Polymer*, vol. 42, no. 4, pp. 1303–1310, 2001.

[14] L. Zhang, X. Gong, Y. Bao et al., "Electrospun nanofibrous membranes surface-decorated with silver nanoparticles as flexible and active/sensitive substrates for surface-enhanced Raman scattering," *Langmuir*, vol. 28, no. 40, pp. 14433–14440, 2012.

[15] Y. L. Li, T. X. Xie, and G. S. Yang, "Effects of polyphenylene oxide content on morphology, thermal, and mechanical properties of polyphenylene oxide/polyamide 6 blends," *Journal of Applied Polymer Science*, vol. 99, no. 5, pp. 2076–2081, 2006.

[16] A. Liu, T. Xie, and G. Yang, "Effect of Na^+-MMT platelets on monomer casting polyamide 6/polyphenylene oxide blends," *Macromolecular Chemistry and Physics*, vol. 207, no. 23, pp. 2180–2187, 2006.

[17] J. E. Puskas, Y. Kwon, V. Altstädt, and M. Kontopoulou, "Blends of poly(2,6-dimethyl-1,4-phenylene oxide) (PPO) with polystyrene-based thermoplastic rubbers: a comparative study," *Polymer*, vol. 48, no. 2, pp. 590–597, 2007.

[18] S. C. Jana, N. Patel, and D. Dharaiya, "Compatibilization of PBT-PPE blends using low molecular weight epoxy," *Polymer*, vol. 42, no. 21, pp. 8681–8693, 2001.

[19] R. T. Tol, G. Groeninckx, I. Vinckier, P. Moldenaers, and J. Mewis, "Phase morphology and stability of co-continuous (PPE/PS)/PA6 and PS/PA6 blends: effect of rheology and reactive compatibilization," *Polymer*, vol. 45, no. 8, pp. 2587–2601, 2004.

[20] Z. Safidine, S. Fellahi, and A. Frick, "Crystallization behavior of PP/PP-g-MAH/GFR PA66 blends: establishment of their continuous-cooling-transformation of relative crystallinity diagrams," *Journal of Applied Polymer Science*, vol. 104, no. 3, pp. 1620–1626, 2007.

[21] C. Q. Li, Y. Zhang, and Y. X. Zhang, "Rheological and mechanical properties of PC/HDPE/glass fiber composites," *Polymers & Polymer Composites*, vol. 10, no. 8, pp. 619–626, 2002.

[22] C.-R. Chiang and F.-C. Chang, "Polymer blends of polyamide-6 (PA6) and poly(phenylene oxide) (PPO) compatibilized by styrene-maleic anhydride (SMA) copolymer," *Polymer*, vol. 38, no. 19, pp. 4807–4817, 1997.

[23] C.-R. Chiang and F.-C. Chang, "Polymer blends of polyamide-6 and poly(phenylene oxide) compatibilized by styrene-co-glycidyl methacrylate," *Journal of Applied Polymer Science*, vol. 61, no. 13, pp. 2411–2421, 1996.

[24] D. Z. Wu, X. D. Wang, and R. G. Jin, "Toughening of poly(2,6-dimethyl-1,4-phenylene oxide)/nylon 6 alloys with functionalized elastomers via reactive compatibilization: morphology, mechanical properties, and rheology," *European Polymer Journal*, vol. 40, no. 6, pp. 1223–1232, 2004.

[25] B. Li, C. Wan, Y. Zhang, and J. Ji, "Blends of poly(2,6-dimethyl-1,4-phenylene oxide)/polyamide 6 toughened by maleated polystyrene-based copolymers: mechanical properties, morphology, and rheology," *Journal of Applied Polymer Science*, vol. 115, no. 6, pp. 3385–3392, 2010.

[26] B. Li, C. Wan, Y. Zhang, J. Ji, and Y. Su, "Reactive compatibilization and elastomer toughening of poly(2,6-dimethyl-1,4-phenylene oxide)/polyamide 6 blends," *Polymers & Polymer Composites*, vol. 18, no. 4, pp. 219–226, 2010.

[27] Y. Son and S. Lee, "One step method for fabrication of PPO/PA-66/elastomer blends," *Polymer Bulletin*, vol. 56, no. 2-3, pp. 267–273, 2006.

[28] K.-C. Chiou, S.-C. Wu, H.-D. Wu, and F.-C. Chang, "Compatibilization and elastomer toughening of polyamide-6 (PA6)/poly(phenylene ether) (PPE) blends," *Journal of Applied Polymer Science*, vol. 74, no. 1, pp. 23–32, 1999.

[29] S. P. Jang and D. Kim, "Thermal, mechanical, and diffusional properties of nylon 6/ABS polymer blends: compatibilizer effect," *Polymer Engineering and Science*, vol. 40, no. 7, pp. 1635–1642, 2000.

[30] D. García-López, S. López-Quintana, I. Gobernado-Mitre, J. C. Merino, and J. M. Pastor, "Study of melt compounding conditions and characterization of polyamide 6/metallocene ethylene-polypropylene-diene copolymer/maleated ethylene-polypropylene-diene copolymer blends reinforced with layered silicates," *Polymer Engineering & Science*, vol. 47, no. 7, pp. 1033–1039, 2007.

[31] R. Gallego, D. García-López, S. López-Quintana, I. Gobernado-Mitre, J. C. Merino, and J. M. Pastor, "Influence of blending sequence on micro- and macrostructure of PA6/mEPDM/EPDMgMA blends reinforced with organoclay," *Journal of Applied Polymer Science*, vol. 109, no. 3, pp. 1556–1563, 2008.

[32] J. Chen, J.-W. Chen, H.-M. Chen, J.-H. Yang, C. Chen, and Y. Wang, "Effect of compatibilizer and clay on morphology and fracture resistance of immiscible high density polyethylene/polyamide 6 blend," *Composites Part B: Engineering*, vol. 54, no. 1, pp. 422–430, 2013.

[33] N. Hasegawa, H. Okamoto, M. Kawasumi, M. Kato, A. Tsukigase, and A. Usuki, "Polyolefin-clay hybrids based on modified polyolefins and organophilic clay," *Macromolecular Materials and Engineering*, vol. 280-281, pp. 76–79, 2000.

[34] L. Jiang, J. W. Zhang, and M. P. Wolcott, "Comparison of polylactide/nano-sized calcium carbonate and polylactide/montmorillonite composites: reinforcing effects and toughening mechanisms," *Polymer*, vol. 48, no. 26, pp. 7632–7644, 2007.